# Numerical simulation of long-range open quantum many-body dynamics with tree tensor networks

Dominik Sulz[1], Christian Lubich[1], Gianluca Ceruti,[2] Igor Lesanovsky[3,4] and Federico Carollo[3]

[1]*Mathematisches Institut, Universität Tübingen, Auf der Morgenstelle 10, D-72076 Tübingen, Germany*

[2]*Institute of Mathematics, EPF Lausanne, 1015 Lausanne, Switzerland*

[3]*Institut für Theoretische Physik, Universität Tübingen, Auf der Morgenstelle 14, 72076 Tübingen, Germany*

[4]*School of Physics and Astronomy and Centre for the Mathematics and Theoretical Physics of Quantum Non-Equilibrium Systems, The University of Nottingham, Nottingham, NG7 2RD, United Kingdom*

Open quantum systems provide a conceptually simple setting for the exploration of collective behavior stemming from the competition between quantum effects, many-body interactions, and dissipative processes. They may display dynamics distinct from that of closed quantum systems or undergo nonequilibrium phase transitions which are not possible in classical settings. However, studying open quantum many-body dynamics is challenging, in particular, in the presence of critical long-range correlations or long-range interactions. Here, we make progress in this direction and introduce a numerical method for open quantum systems, based on tree tensor networks. Such a structure is expected to improve the encoding of many-body correlations and we adopt an integration scheme suited for long-range interactions and applications to dissipative dynamics. We test the method using a dissipative Ising model with power-law decaying interactions and observe signatures of a first-order phase transition for power-law exponents smaller than 1.

## I. INTRODUCTION

The interaction of a quantum system with its surroundings induces dissipative effects which require the description of its state in terms of density matrices. In the simplest case, these matrices evolve through Markovian quantum master equations [1–3]. However, solving these equations for many-body systems is a daunting task, especially beyond noninteracting theories [4–8]. This is due to the exponential growth (with the system size) of the resources needed to encode quantum states, which seriously limits the investigation of nonequilibrium behavior in open quantum systems [9–20].

To overcome this limitation, several numerical approaches have been developed [21–26], including techniques based on neural networks [27–32]. At least for one-dimensional quantum systems, the state-of-the-art methodology is based on matrix product states (MPSs) [33–41], despite open questions on their performance for open quantum dynamics [23] and on error bounds for the estimation of expectation values. These aspects are particularly relevant close to nonequilibrium phase transitions, where MPS methods can become unstable [14,16] since they struggle to capture long-range correlations in critical systems or in systems with long-range interactions.

Recently, tree tensor networks (TTNs), which are tensor networks featuring both a physical and several hidden layers [see sketch in Fig. 1(a)], have been successfully employed to encode critical long-range correlations [42] in Hamiltonian systems [43–47] (see also Refs. [48–51] for other applications). This enhanced capability is rooted in their structure [cf. Fig. 1(a)], which is such that the number of tensors between two subsystems scales only logarithmically with their distance [43] and not linearly as for MPSs. Despite this feature, TTNs have not yet been used for simulating critical or long-range

open quantum dynamics [26] (see, however, related ideas in Refs. [52–54]).

In this paper, we present an algorithm for simulating quantum master equations which exploits a TTN representation of quantum many-body states. Our approach, based on the integration scheme put forward in Ref. [55], evolves a TTN by a hierarchical "basis update and Galerkin" (BUG) method. It first updates the orthonormal basis matrices which are found at the *leaves* of the tree and then evolves the *connecting tensors* within the hidden layers [see Fig. 1(a)] by a variational or Galerkin method.

To benchmark our algorithm, we consider a paradigmatic open quantum system, the dissipative Ising model sketched in Fig. 1(b), in the presence of power-law decaying interactions. We show the validity of the method by checking it against (numerically) exact results for both short-range and long-range interactions and we investigate signatures of a first-order phase transition in the long-range scenario. We further consider a global "susceptibility" observable and explore how TTNs perform in describing many-body correlations. Our results indicate that TTNs are promising for simulating open quantum many-body systems in the presence of long-range interactions.

## II. OPEN QUANTUM DYNAMICS

We consider one-dimensional quantum systems consisting of $D$ distinguishable $d$-level particles undergoing Markovian open quantum dynamics. The density matrix $\rho(t)$ describing the state of the system evolves through the quantum master equation [1–3]

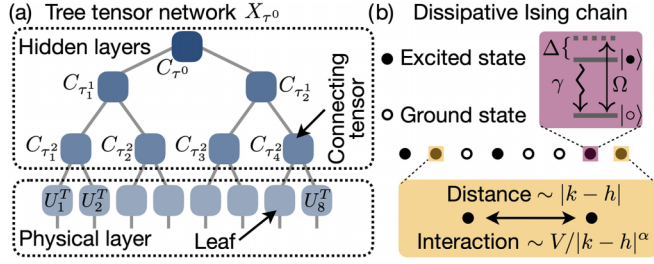$$\dot{\rho}(t) = \mathcal{L}[\rho(t)] := -i[H, \rho(t)] + \mathcal{D}[\rho(t)]. \tag{1}$$

FIG. 1. Tree tensor networks and dissipative Ising model. (a) Binary tree tensor network $X_{\tau^0}$ living on a tree $\tau^0$, associated with a system made by $D = 8$ particles. The network consists of a physical layer, containing the leaves of the tree (each one related to a particle), and three hidden layers. The hidden layers are made by connecting tensors $C_{\tau_i^j}$, pairwise joining elements from the previous layer. (b) Dissipative Ising model with two-level subsystems and single-particle states $|\bullet\rangle$, $|\circ\rangle$. The system Hamiltonian drives coherent oscillations between states $|\bullet\rangle \leftrightarrow |\circ\rangle$ with Rabi frequency $\Omega$ and detuning $\Delta$. The irreversible process consists of local decay $|\bullet\rangle \rightarrow |\circ\rangle$ with rate $\gamma$. Two subsystems in state $|\bullet\rangle$ interact with a strength depending on the parameter $V$ and on their distance through the interaction-range exponent $\alpha$.

The map $\mathcal{L}$ is the Lindblad dynamical generator and $H = H^\dagger$ is the many-body Hamiltonian operator. The dissipator $\mathcal{D}$ assumes the form

$$\mathcal{D}[\rho] = \sum_\mu \left( J_\mu \rho J_\mu^\dagger - \frac{1}{2}\{\rho, J_\mu^\dagger J_\mu\} \right), \qquad (2)$$

with the jump operators $J_\mu$ encoding how the environment affects the system dynamics.

The Lindblad generator in Eq. (1) is a linear map from the space of matrices onto itself. To numerically simulate open quantum dynamics, it is convenient to represent $\mathcal{L}$ as a matrix acting on a vectorized representation of matrices (see, e.g., Refs. [16,56–58]). Any matrix $\rho(t)$ thus becomes a vector $|\rho(t)\rangle$, and Eq. (1) reads

$$|\dot{\rho}(t)\rangle = \mathbb{L}|\rho(t)\rangle, \qquad (3)$$

with $\mathbb{L}$ being the matrix representation of the generator $\mathcal{L}$ (see Appendix A for an example). In what follows, we show how the solution of Eq. (3) can be approximated by means of TTNs.

## III. INTEGRATION WITH TREE TENSOR NETWORKS

TTNs feature a physical layer and several hidden layers [cf. Fig. 1(a)], which we exploit to store the physical data corresponding to the quantum state $|\rho(t)\rangle$. The leaves of the tree, i.e., the tensors (in fact, matrices) in the physical layer, correspond to the sites of our one-dimensional quantum system while the connecting tensors in the hidden layers encode the correlations between them. To approximate the open quantum dynamics, we adopt an algorithm [55] that decomposes the Dirac-Frenkel time-dependent variational principle [59–61] for TTNs into computable discrete time steps, variationally evolving each tensor of the TTN in a hierarchical order from the leaves to the root (bottom-up). A single update of the algorithm consists of two steps:

(1) Construct a state-dependent reduction $L_{\tau_i^j}$ of the Lindblad generator for each tensor in layer $j$,

(2) Update the tensor variationally, by solving the system of differential equations implemented by $L_{\tau_i^j}$,

which are repeated recursively going from the bottom to the top layer. We now provide a concise description of the algorithm and refer to Ref. [55] for details.

The physical layer is formed by $D = 2^\ell$ leaves, each one associated with a site of the system. Each leaf is the smallest possible subtree, which we call $\tau_i^\ell$, see Fig. 2(a). The superscript $\ell$ labels the (physical) layer to which the leaf belongs, while $i$, for $i = 1, 2, \ldots, D$, denotes the leaf itself. The tensor associated with each leaf is a complex matrix $U_i$, with orthonormal columns and dimensions $d^2 \times r_{\tau_i^\ell}$, carrying a physical basis. We will use the letter $r$ to denote bond dimensions within the TTN.

Proceeding towards the root (top) of the tree depicted in Fig. 1(a), for each hidden layer $j$ we can recursively define larger subtrees $\tau_i^j$ obtained by joining subtrees from the previous layer, namely, $\tau_i^j = (\tau_{2i-1}^{j+1}, \tau_{2i}^{j+1})$ [cf. Fig. 2(a)]. Each subtree is related to a tensor network $X_{\tau_i^j}$, at the root of which one finds the connecting tensor $C_{\tau_i^j}$, with dimension $r_{\tau_i^j} \times r_{\tau_{2i-1}^{j+1}} \times r_{\tau_{2i}^{j+1}}$. As shown in Fig. 2(b), the first index of these tensors (bond dimension $r_{\tau_i^j}$) points upward and is counted as the zeroth dimension, followed by the second and third indices (bond dimensions $r_{\tau_{2i-1}^{j+1}}$ and $r_{\tau_{2i}^{j+1}}$) which point downward to the left and right subtree, respectively.

We further define the tensor-matrix multiplication $A = C \times_m B$, between an order-$n$ tensor $C$ and a matrix $B$ with respect to $m$th tensor index as [see, e.g., Fig. 2(c)]

$$A_{k_0,k_1,\ldots,k_m,\ldots,k_{n-1}} = \sum_{\ell_m} C_{k_0,k_1,\ldots,\ell_m\ldots,k_{n-1}}(B^T)_{\ell_m,k_m}, \qquad (4)$$

as well as the *matricization* of a tensor $\text{Mat}_i(C) = C_i \in \mathbb{C}^{r_i \times r_i'}$, where $r_i' = \prod_{j \neq i} r_j$, with inverse operation, $\text{Ten}_i(C_i) = C$, called *tensorization* [cf. Fig. 2(c)]. We work with orthonormal TTNs, for which $\text{Mat}_0(C)^T$ has orthonormal columns for each connecting tensor $C$, with the exception of the connecting tensor $C_{\tau^0}$ at the root (top). The relation $r_i \leqslant \prod_{j \neq i} r_j$ must be satisfied for $i = 0, 1, 2$, to ensure that each matricization of each connecting tensor $C$ can be (and usually is) of full rank.

To obtain the evolved TTN over a discrete (infinitesimal) time-step $\delta t$, we need to find the updated leaves $U_i'$ and the updated connecting tensors $C_{\tau_i^j}'$. In the algorithm, we first update the basis matrices $U_i$ at the leaves. To this end, we take the connecting tensor above the leaf $\tau_i^\ell$ that needs to be updated, $C = C_{\tau_{\lceil i/2 \rceil}^{\ell-1}}$, matricize it as $C_1 = \text{Mat}_1(C)$ if $i$ is odd or as $C_2 = \text{Mat}_2(C)$ if $i$ is even. We then perform a QR decomposition $C_i^T = Q_i R_i$, with $R_i$ having dimension $r_i \times r_i$, and define the matrix $Y_i = R_i U_i^T$. This provides the initial condition, $Y_i(0) = Y_i$, for the matrix differential equation

$$\dot{Y}_i = L_{\tau_i^\ell}[Y_i]. \qquad (5)$$

The linear operator $L_{\tau_i^\ell}$ can be interpreted as a state-dependent variational reduction to the $i$th physical site of the Lindblad operator and, as we discuss below, is defined recursively. Solving the differential equation up to time $\delta t$, we find $Y_i(\delta t)$
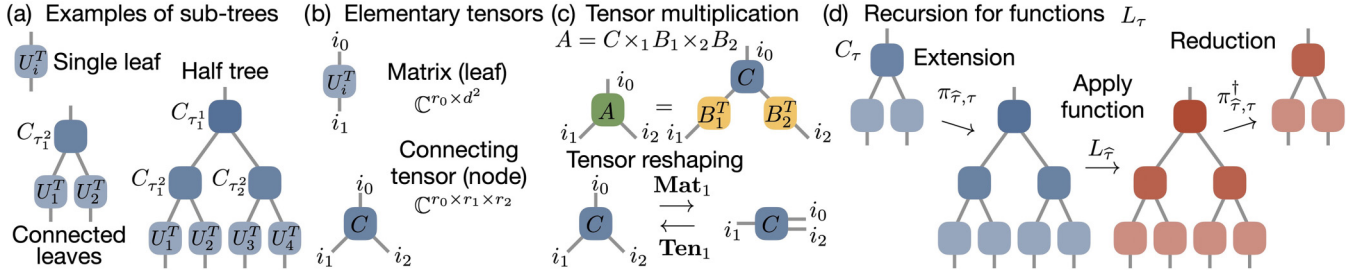
FIG. 2. Tree tensor networks: subtrees and operations. (a) Examples of tensor networks $X_\tau$, defined on subtrees of the TTN shown in Fig. 1(a). Apart from the leaves, each $X_\tau$ has a connecting tensor $C_\tau$ at the top. (b) Leaves are complex orthogonal matrices with dimension $r_0 \times d^2$, where $d$ is the dimension of the single-particle Hilbert space. Connecting tensors are order-three tensors with bond dimension $r_0 \times r_1 \times r_2$. The indexes of the tensors are numbered from 0 to $M - 1$, where $M$ is the order of the tensor. (c) Sketch of the tensor multiplication [cf. Eq. (4)] and of the reshaping functions $\mathrm{Mat}_i$, $\mathrm{Ten}_i$, shown for $i = 1$. (d) Recursion algorithm for finding $L_\tau$. Given $L_{\hat\tau}$, with $\hat\tau$ being the smallest tree larger than $\tau$ and containing it, to find $L_\tau$ we extend the tensor network $X_\tau$ to a tensor network on the larger tree $\hat\tau$, via the operation $\pi_{\hat\tau,\tau}$. We apply the function $L_{\hat\tau}$ on the extended tensor network and then reduce the resulting tensor back to $\tau$ through $\pi_{\hat\tau,\tau}^\dagger$.

and set the updated leaf matrix $U_i'$ as the orthogonal part of the QR factorization of $Y_i(\delta t)$.

We then hierarchically update the connecting tensors from the bottom to top layer. At each step of the recursion, we set $\widehat{C}_{\tau_i^j} = C_{\tau_i^j} \times_1 M_{\tau_{2i-1}^{j+1}} \times_2 M_{\tau_{2i}^{j+1}}$ [cf. Fig. 2(c)], with $M_\tau = U_\tau'^\dagger U_\tau$, where $U_\tau = \mathrm{Mat}_0(X_\tau)^T$ is the matricization of $X_\tau$. When $\tau$ is a leaf, $\tau = \tau_i^\ell$, then $U_{\tau_i^\ell} = U_i$. The matrices $U_\tau'$ are defined analogously but for the already updated $X_\tau'$ (see also Appendix B). The tensor $\widehat{C}_{\tau_i^j}$ provides the initial data for the differential equation

$$\dot{\widehat{C}}_{\tau_i^j} = L_{\tau_i^j}\left[\widehat{C}_{\tau_i^j} \times_1 U_{\tau_{2i-1}^{j+1}}' \times_2 U_{\tau_{2i}^{j+1}}'\right] \times_1 U_{\tau_{2i-1}^{j+1}}'^\dagger \times_2 U_{\tau_{2i}^{j+1}}'^\dagger. \quad (6)$$

The updated tensor is $C_{\tau_i^j}' = \mathrm{Ten}_0(Q^T)$, where $Q$ is the orthogonal part of the QR decomposition of $\mathrm{Mat}_0(\widehat{C}_{\tau_i^j}(\delta t))^T$. Note that the matrices $U_\tau$, $U_\tau'$ are never explicitly constructed since the products involving them are computed by contracting corresponding TTNs.

Finally, we discuss how the reduced Lindblad operators $L_{\tau_i^j}$ can be obtained (see Refs. [62] and Appendix B for details). For any subtree $\tau$, $L_\tau$ can be found from the knowledge of $L_{\hat\tau}$ associated with the smallest subtree $\hat\tau$ containing $\tau$. By defining a state-dependent extension operator $\pi_{\hat\tau,\tau}$, which maps the tree $\tau$ into the larger tree $\hat\tau$, the operator $L_\tau$ is given by $L_\tau = \pi_{\hat\tau,\tau}^\dagger L_{\hat\tau} \pi_{\hat\tau,\tau}$. The starting point of the recursion is given by $L_{\tau^0}$, related to the entire tree $\tau^0$, which is nothing but a (possibly truncated) TTN-operator representation of the matrix $\mathbb{L}$.

The integrator presented above [55], which extends the BUG matrix integrators of Refs. [63,64] does not have any backward-in-time propagation in contrast to those of Refs. [37,38,62]. This makes it better suited for the simulation of dissipative dynamics.

## IV. LONG-RANGE DISSIPATIVE ISING MODEL

To benchmark our algorithm, we consider a long-range interacting version of the dissipative Ising model [21,67–75]. It consists of a one-dimensional model with two-level particles, characterized by the excited state $|\bullet\rangle$ and ground state $|\circ\rangle$. The

model Hamiltonian [cf. Fig. 1(b)] is given by

$$H = \Omega \sum_{k=1}^{D} \sigma_x^{(k)} + \Delta \sum_{k=1}^{D} n^{(k)} + \frac{V}{2c_\alpha} \sum_{k\neq h=1}^{D} \frac{n^{(k)}n^{(h)}}{|k - h|^\alpha}, \quad (7)$$

where $n = |\bullet\rangle\langle\bullet|$ and $\sigma_x = |\bullet\rangle\langle\circ| + |\circ\rangle\langle\bullet|$. The first two terms in the above equation describe a driving term, e.g., from a laser, with Rabi frequency $\Omega$ and detuning $\Delta$. The last term describes two-body interactions solely occurring between particles in the excited state $|\bullet\rangle$. The parameter $V$ is an overall coupling strength while the algebraic exponent $\alpha$ controls the range of the interactions. For $\alpha = 0$ the interaction is of all-to-all type while for $\alpha \to \infty$ it only involves nearest neighbors. The coefficient $c_\alpha = \sum_{k=1}^{D} 1/k^\alpha$ keeps the interaction extensive for any value of $\alpha$ [76–78]. Dissipation [cf. Eq. (2)] is encoded in the jump operators $J_k = \sqrt{\gamma}\sigma_-^{(k)}$, where $\sigma_- = |\circ\rangle\langle\bullet|$ describes irreversible decay from state $|\bullet\rangle$ to state $|\circ\rangle$. In the following, we shall consider as initial state the state with all particles in $|\bullet\rangle$.

### A. Benchmark of the TTN algorithm

To show that our algorithm faithfully approximates the open quantum dynamics, we test our results for different values of $\alpha$. When $\alpha = 0$, we check our numerics against an efficient diagonalization method for the generator, possible for permutation-invariant systems [79–82]. For $\alpha \to \infty$, we compare numerical results with those obtained using MPSs and a time-evolving-block-decimation (TEBD) algorithm [24,33,34,39,83]. For $0 < \alpha < \infty$, we can only benchmark our results against a standard exact diagonalization of the Lindblad generator, possible for relatively small systems. As shown in Figs. 3(a) and 3(b), the results from our TTN algorithm agree with the corresponding reference solutions.

### B. Role of the interaction range

We now exploit our algorithm to explore the behavior of the system for intermediate values of $\alpha$ and larger system sizes. Such a regime is of interest for at least two reasons. First, values such as $\alpha = 3$ or $\alpha = 6$ are typically encountered in experiments [84]. Second, for $\alpha = 0$ and in the
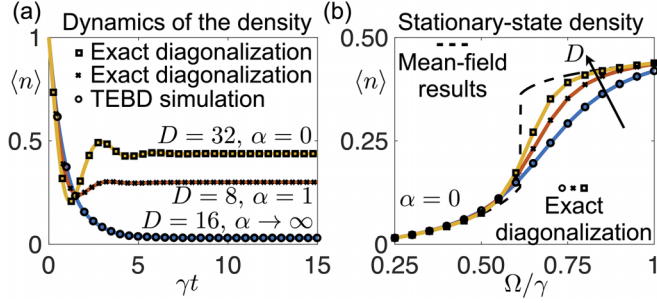
FIG. 3. Benchmark of the method. (a) Time evolution of the density $\langle n \rangle$ computed with our algorithm (solid lines) and other approaches (symbols). For the nearest-neighbor interacting case ($D = 16$, $\alpha \to \infty$), we benchmark our results against converged MPS simulations with a time-evolving-block-decimation (TEBD) algorithm. For $D = 8$, $\alpha = 1$ and $D = 32$, $\alpha = 0$, we compare with results obtained with exact diagonalization of the Lindblad generator. For our simulations we used a maximal bond dimension $r_{\max} = 30$. We consider $\Omega/\gamma = 0.3, 0.7, 1$, respectively, for the different curves. (b) Stationary values of the density as a function of $\Omega/\gamma$, obtained by evolving up to $\gamma t = 15$ the TTNs and exact-diagonalization simulations. Here, we show the infinite-range interacting case ($\alpha = 0$) for system sizes $D = 8, 16, 32$, for which we use maximal bond dimension $r_{\max} = 10, 20, 30$, respectively. The dashed-line shows the mean-field prediction, which is exact for $D \to \infty$ [65,66]. The parameters not explicitly specified in the panels are $\Delta/\gamma = -2$, $V/\gamma = 5$.

thermodynamic limit $D \to \infty$, the dissipative Ising model features a first-order nonequilibrium phase transition from a phase with a low density of excitations $\langle n \rangle$ to a highly excited one [cf. dashed line in Fig. 3(b)]. On the other hand, for $\alpha \to \infty$ the transition is not present in the one-dimensional model [71]. Our TTN algorithm can interpolate between these two regimes and allows us to explore the fate of the transition for $\alpha > 0$. In Fig. 4(a), we see that for $\alpha > 1$ the stationary
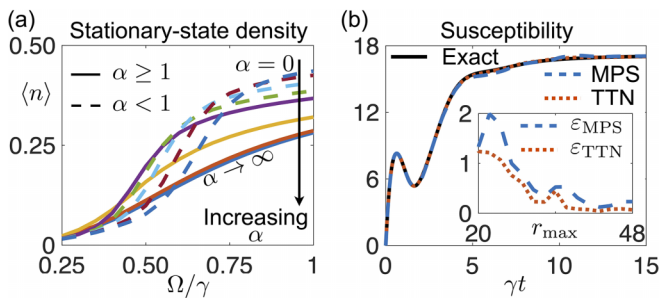


FIG. 4. Long-range interactions and "susceptibility" parameter. (a) Stationary behavior of the density $\langle n \rangle$ as a function of $\Omega/\gamma$ for different values of $\alpha$ and $D = 16$, as estimated at $\gamma t = 15$. We consider $\alpha = 0, 0.25, 0.50, 0.75, 1, 2, 5$ and $\alpha \to \infty$, growing as denoted in the plot. For all values of $\alpha$, we consider $r_{\max} = 30$ but for $\alpha = 0$, for which $r_{\max} = 20$ is sufficient. (b) Dynamics of the susceptibility $\chi$ for $\Omega/\gamma = 0.65$, for both TTN and MPS simulations with $r_{\max} = 38$ and $D = 32$. The TTN curve essentially coincides with the exact solution while the MPS curve still shows some deviation. The inset displays the maximal errors $\varepsilon_{\text{TTN/MPS}}$ in estimating $\chi$ as a function of the bond dimension. The parameters not explicitly specified in the panels are $\Delta/\gamma = -2$, $V/\gamma = 5$.

density $\langle n \rangle$ behaves similarly to the case $\alpha \to \infty$, i.e., there appears to be a smooth behavior of the density $\langle n \rangle$ as a function of $\Omega/\gamma$. On the other hand, for $\alpha \leqslant 1$ for which the sum of the interaction terms in Eq. (7), without considering $c_\alpha$, would become superextensive, we observe the emergence of a sharp crossover which is reminiscent of what happens in the $\alpha = 0$ case.

To assess the capability of TTNs to capture correlations, we also consider the total density fluctuations in the system $\chi = \sum_{k,h=1}^{D} (\langle n^{(k)} n^{(h)} \rangle - \langle n^{(k)} \rangle \langle n^{(h)} \rangle)$. This quantity, which is highly nonlocal as it contains all possible two-body density-density correlations, represents a susceptibility parameter. Here, we focus on the case $\alpha = 0$, for which we can obtain exact results for larger systems [79–82], and compare results for TTNs and MPSs. MPS simulations are also performed using our algorithm for a TTN of maximal height, which is equivalent to the MPS ansatz [55]. In Fig. 4(b), we display simulations with a same, relatively large, bond dimension for TTNs and MPSs. The plot shows that the TTN results are almost perfectly overlapping with the exact values of the susceptibility, while deviations can still be appreciated in the MPS simulations. In the inset of Fig. 4(b), we show the errors $\varepsilon_{\text{TTN/MPS}} = \max_{\gamma t \in [0,15]} |\chi_{\text{TTN/MPS}} - \chi|$, where $\chi$ is the exact susceptibility, while $\chi_{\text{TTN/MPS}}$ the value estimated with TTNs and MPSs, respectively. Already for the simple all-to-all ($\alpha = 0$) interaction considered, which does not develop critical long-range correlations since it features a first-order transition in the thermodynamic limit, we can observe that TTNs perform systematically better than MPSs. More precisely, we observe, in the inset of Fig. 4(b), that TTNs describe more accurately than MPSs the behavior of the susceptibility for a same bond dimension.

### C. Computational cost

The most time-consuming parts of our numerical simulations are: (i) the applications of the TTN-operator to the TTN-representations of the state; (ii) the computation of the state-dependent extension operator [cf. Fig. 2(d)] needed for the construction of the subfunctions $L_\tau$ from Appendix B. In particular, for a single time-step we need $\mathcal{O}(D)$ applications of the TTNO, with the actual number depending on the chosen method to solve the differential equations (5) and (6). As stated in lemma 4.1 of Ref. [55], performing a complete time step with our integrator requires $\mathcal{O}[\ell D^2 r_{\max}^2 (d^2 + r_{\max}^3)]$ arithmetical operations, where $\ell$ denotes the number of layers of the TTN [see sketch in Fig. 1(a)], $D$ the number of particles, $r_{\max}$ the maximal bond dimension and $d$ the physical single-site dimension. In our implementation, the constant $\ell$ scales linearly for MPS (we note that MPSs correspond to trees of maximal height), while it only scales logarithmically with $D$ for TTNs. In practice, we observe that the runtime for each dynamical simulation was, on average, of the order of a few days.

### V. CONCLUSION

We introduced a method for the numerical simulation of long-range open quantum systems with TTNs and benchmarked it considering the paradigmatic dissipative Ising model. With our method, we could explore the regime of

intermediate interaction ranges where we found signatures of the persistence of the phase transition for $\alpha \in [0, 1]$ in the thermodynamic limit. We also tested the capability of TTNs to encode correlations. We found that for the considered system, TTNs perform better than simulations with MPSs. Our simulations were performed using standard PCs.

As a future perspective, it would be interesting to compare the two approaches for open quantum systems featuring second-order nonequilibrium phase transitions and a critical building-up of correlations [14]. It would also be relevant to explore different tree structures. Here, we mainly considered balanced binary trees and MPSs, but the algorithm is general and applies to any tree [55]. This opens up the possibility of a systematic investigation on the role of the tree structure in the encoding of many-body correlations for extended open quantum systems.

### APPENDIX A: MATRIX REPRESENTATION OF THE LINDBLAD GENERATOR

We show here how the time evolution of the density matrix $\rho(t)$ can be formulated in terms of a vector differential equation. For the sake of concreteness, we focus on the case of the dissipative Ising model discussed in the main text for which the time evolution of the density matrix is given by the Lindblad equation

$$\dot{\rho}(t) = -i[H, \rho(t)] + \sum_{k=1}^{D} \gamma \left( \sigma_{-}^{(k)} \rho(t) \sigma_{+}^{(k)} - \frac{1}{2}\{\rho(t), n^{(k)}\} \right).$$

For this model, we have the single-particle basis states $|\bullet\rangle, |\circ\rangle$, with which we can define $\sigma_{-} = |\circ\rangle\langle\bullet|$, $\sigma_{+} = \sigma_{-}^{\dagger}$ and $n = |\bullet\rangle\langle\bullet|$. The system Hamiltonian is

$$H = \Omega \sum_{k=1}^{D} \sigma_x^{(k)} + \Delta \sum_{k=1}^{D} n^{(k)} + \frac{V}{2c_\alpha} \sum_{k \neq h=1}^{D} \frac{n^{(k)} n^{(h)}}{|k - h|^\alpha}, \quad \text{(A1)}$$

with $\sigma_x = \sigma_- + \sigma_+$.

The starting point of the mapping of the above matrix equation into a vector one is to take the density matrix $\rho(t)$, and write it as a vector in an enlarged single-particle Hilbert space. This can be achieved, for instance, through the following mapping $\rho(t) \rightarrow |\rho(t)\rangle$ with

$$\rho(t) = \sum_{\vec{\ell}, \vec{m}} r_{\vec{\ell}\vec{m}}(t) |\vec{\ell}\rangle\langle\vec{m}|$$

and

$$|\rho(t)\rangle = \sum_{\vec{\ell}, \vec{m}} r_{\vec{\ell}\vec{m}}(t) \bigotimes_{k=1}^{D} [|\ell_k\rangle \otimes |m_k\rangle].$$

Here, we have that $\vec{\ell} = (\ell_1, \ell_2, \dots \ell_D)$ and $\vec{m} = (m_1, m_2, \dots, m_D)$ are many-body configuration states, where $\ell_k, m_k = \bullet, \circ$ specify the single-particle state. In this representation, the Lindblad generator is given by the following matrix:

$$\mathbb{L} = \gamma \sum_{k=1}^{D} \left( \sigma_{-,\mathrm{I}}^{(k)} \sigma_{-,\mathrm{II}}^{(k)} - \frac{1}{2} n_{\mathrm{I}}^{(k)} - \frac{1}{2} n_{\mathrm{II}}^{(k)} \right)$$
$$- i \sum_{k=1}^{D} \Omega \left( \sigma_{x,\mathrm{I}}^{(k)} - \sigma_{x,\mathrm{II}}^{(k)} \right) + -i \sum_{k \neq h}^{D} \frac{V}{2c_\alpha |k - h|^\alpha}$$
$$\times \left( n_{\mathrm{I}}^{(k)} n_{\mathrm{I}}^{(h)} - n_{\mathrm{II}}^{(k)} n_{\mathrm{II}}^{(h)} \right), \quad \text{(A2)}$$

where $\sigma_{-,\mathrm{I}} = \sigma_- \otimes \mathbf{1}_2$, $\sigma_{-,\mathrm{II}} = \mathbf{1}_2 \otimes \sigma_-$ and similarly, $\sigma_{x,\mathrm{I}} = \sigma_x \otimes \mathbf{1}_2$, $\sigma_{x,\mathrm{II}} = \mathbf{1}_2 \otimes \sigma_x$ as well as $n_{\mathrm{I}} = n \otimes \mathbf{1}_2$, $n_{\mathrm{II}} = \mathbf{1}_2 \otimes n$ and $\mathbf{1}_2$ is the $2 \times 2$ identity. Note that, in principle, one should have transposition of all the terms denoted with II in the above Eq. (A2), exception made for those in the first term of the first sum (see also, e.g., Refs. [16,58]). However, in our case all the matrices involved are already self-transposed. The time evolution is thus implemented via the vectorized differential equation

$$|\dot{\rho}(t)\rangle = \mathbb{L}|\rho(t)\rangle.$$

To conclude we recall how expectation values can be computed within this vectorized formalism. Let us consider an elementary operator

$$O = \bigotimes_{k=1}^{D} x_k,$$

where $x_k$ are $2 \times 2$ matrices. Then, its expectation value can be computed as

$$\langle O \rangle_t = \langle -| \bigotimes_{k=1}^{D} x_{k,\mathrm{I}}^{(k)} |\rho(t)\rangle,$$

where we defined $x_{k,\mathrm{I}} = x_k \otimes \mathbf{1}_2$ as well as the vector representation of the identity

$$|-\rangle = \bigotimes_{k=1}^{D} |\mathbf{1}_2\rangle,$$

with $|\mathbf{1}_2\rangle = |\bullet\rangle \otimes |\bullet\rangle + |\circ\rangle \otimes |\circ\rangle$. In the main text, we always considered as initial state the state

$$|\rho(0)\rangle = \bigotimes_{k=1}^{D} (|\bullet\rangle \otimes |\bullet\rangle).$$

### APPENDIX B: ADDITIONAL DETAILS ON THE TREE TENSOR NETWORK ALGORITHM

#### 1. Recursive definition of a tree tensor network

Suppose to be given a set of basis matrices $U_j$ for $j = 1, \dots, D$ and of the connecting tensors $C_{\tau_i^j}$ for all subtrees

$\tau_i^j$ of $\tau^0$. We recursively define a tree tensor network $X_{\tau^0}$ as follows.

(i) For each leaf, we set

$$X_j := U_j^T \in \mathbb{C}^{r_j \times n_j}.$$

(ii) For each subtree $\tau_i^j = (\tau_{2i-1}^{j+1}, \tau_{2i}^{j+1})$ of the maximal tree $\tau^0$, we set $n_{\tau_i^j} = n_{\tau_{2i-1}^{j+1}} n_{\tau_{2i}^{j+1}}$ and

$$X_{\tau_i^j} := C_{\tau_i^j} \times_1 U_{\tau_{2i-1}^{j+1}} \times_2 U_{\tau_{2i}^{j+1}} \in \mathbb{C}^{r_{\tau_i^j} \times n_{\tau_{2i-1}^{j+1}} \times n_{\tau_{2i}^{j+1}}},$$

$$U_{\tau_i^j} := \mathrm{Mat}_0\big(X_{\tau_i^j}\big)^T \in \mathbb{C}^{n_{\tau_i^j} \times r_{\tau_i^j}}.$$

### 2. Construction of the $M_\tau$ matrices

The matrix $M_\tau = U_\tau'^\dagger U_\tau$, where $\tau = (\tau_1, \tau_2)$, can be constructed recursively. By definition of a tree tensor network we know that it holds

$$U_\tau' = \mathrm{Mat}_0\big(C_\tau' \times_1 U_{\tau_1}' \times_2 U_{\tau_2}'\big)^T,$$

$$U_\tau = \mathrm{Mat}_0\big(C_\tau \times_1 U_{\tau_1} \times_2 U_{\tau_2}\big)^T,$$

where $U_{\tau_i}'$ and $U_{\tau_i}$, for $i = 1, 2$, are either basis matrices or again a matricized tree tensor network from the level below. Using the unfolding formula for the tree tensor networks (see Eq. (2.2) in Ref. [55]) we obtain

$$M_\tau = U_\tau'^\dagger U_\tau$$

$$= \big(\mathrm{Mat}_0\big(C_\tau' \times_1 U_{\tau_1}' \times_2 U_{\tau_2}'\big)^T\big)^\dagger \mathrm{Mat}_0\big(C_\tau \times_1 U_{\tau_1} \times_2 U_{\tau_2}\big)^T$$

$$= \overline{\mathrm{Mat}_0(C_\tau')}\big(\times_1 U_{\tau_1}'^\dagger U_{\tau_1} \times_2 U_{\tau_2}'^\dagger U_{\tau_2}\big)\mathrm{Mat}_0(C_\tau)^T.$$

The products $U_{\tau_i}'^\dagger U_{\tau_i}$, for $i = 1, 2$, can now be computed recursively until we reach the basis matrices.

### 3. Constructing and applying the tree tensor network operators $L_\tau$

As we showed in the first section of this Appendix, the Lindblad operator can be written, in its matrix representation, as a linear operator of the form

$$\mathbb{A} = \sum_{k=1}^s a_k^1 \otimes \cdots \otimes a_k^D,$$

where $a_k^j$ are complex matrices which act on the $j$th particle. Similar ideas for the construction and application of TTNO's can be found in Ref. [87]. We define the tree tensor network operator $A = L_{\tau^0}$, which acts on a tree tensor network $X_{\tau^0}$, to be the tensor network with the following.

(1) The $j$th leaf equal to the matrix $[\mathbf{vec}(a_1^j), \ldots, \mathbf{vec}(a_s^j)]$, where the $\mathbf{vec}(B)$ denotes the vectorization of the matrix $B$.

(2) All connecting tensors $C_\tau \in \mathbb{C}^{s \times s \times s}$ with entries $C(k_1, k_2, k_3) = 1$ if and only if $k_1 = k_2 = k_3$. Otherwise the entries are zero.

(3) The connecting tensor $C_{\tau^0} \in \mathbb{C}^{s \times s \times 1}$ at the top level with again entries $C_{\tau^0}(k_1, k_2) = 1$ if and only if $k_1 = k_2$, and otherwise zero.

The resulting tree tensor network should be then orthonormalized and possibly truncated to a reasonable bond dimension. We will call this orthonormal TTN $\tilde{A}$. Now we define the application of $\tilde{A}$ to a tree tensor network $X_{\tau^0}$. The leaves and connecting tensors are applied in the following way.

(1) Let $U_j$ be the $j$th leaf of $X_{\tau^0}$. Then the $j$th leaf of $\tilde{A}(X_{\tau^0})$ is defined as the matrix $[\tilde{a}_1^j U_j, \ldots, \tilde{a}_n^j U_j]$, where $\tilde{a}_i^j$ are the matricizations of the $i$th columns of the $j$th leaf of the TTNO $\tilde{A}$.

(2) Let $C_{\tau_i^j}$ be the connecting tensor at $j$th level and $i$th position of $X_{\tau^0}$ and $\tilde{C}_{\tau_i^j}$ the connecting tensor at the $j$th level and $i$th position of $\tilde{A}$. Then the connecting tensor of the application is defined as $\tilde{C}_{\tau_i^j} \otimes C_{\tau_i^j}$, where $\otimes$ denotes the canonical extension of the Kronecker product to tensors.

### 4. Constructing $L_{\tau_i^j}$

Suppose we are given a TTNO $L_{\tau^0}$, constructed as above. Now we are interested in constructing the subfunctions $L_{\tau_i^j}$, which are needed for the algorithm (see main text). The definition of these functions is again done recursively from the root to the leaves.

Suppose that for a tree $\tau = (\tau_1, \tau_2)$ the function $L_\tau$ is already constructed. Let $X_\tau$ be a TTN with connecting tensor $C_\tau$ and matrices $U_{\tau_1} = \mathrm{Mat}_0(X_{\tau_1})^T$ and $U_{\tau_2} = \mathrm{Mat}_0(X_{\tau_2})^T$, i.e., $X_\tau = C_\tau \times_1 U_{\tau_1} \times_2 U_{\tau_2}$. We define the space $\mathcal{V}_\tau = \mathbb{C}^{r_\tau \times n_{\tau_1} \times n_{\tau_2}}$, where $n_\tau = \prod_{i=1}^2 n_{\tau_i}$ is defined recursively. We define the matrices

$$V_{\tau_1}^0 = \mathrm{Mat}_1\big(\mathrm{Ten}_1\big(Q_{\tau_1}^T\big) \times_2 U_{\tau_2}\big)^T,$$

$$V_{\tau_2}^0 = \mathrm{Mat}_2\big(\mathrm{Ten}_2\big(Q_{\tau_2}^T\big) \times_1 U_{\tau_1}\big)^T,$$

where $Q_{\tau_i}$, for $i = 1, 2$, is the unitary factor in the QR decomposition of $\mathrm{Mat}_0(C_{\tau_i})^T = Q_{\tau_i} R_{\tau_i}$ and $C_{\tau_i}$ is the connecting tensor of $X_{\tau_i}$. Further we define two functions

$$\pi_{\tau,i}(Y_{\tau_i}) = \mathrm{Ten}_i\big\{\big[V_{\tau_i}^0 \mathrm{Mat}_0\big(Y_{\tau_i}\big)\big]^T\big\} \in \mathcal{V}_\tau, \quad \text{for } Y_{\tau_i} \in \mathcal{V}_{\tau_i},$$

$$\pi_{\tau,i}^\dagger(Z_\tau) = \mathrm{Ten}_0\big\{\big[\mathrm{Mat}_i(Z_\tau)V_{\tau_i}^0\big]^T\big\} \in \mathcal{V}_{\tau_i}, \quad \text{for } Z_\tau \in \mathcal{V}_\tau.$$

The function $L_{\tau_i}$ now is defined recursively by

$$L_{\tau_i} = \pi_{\tau,i}^\dagger \circ L_\tau \circ \pi_{\tau,i}, \quad \text{for } i = 1, 2. \tag{B1}$$

[1] G. Lindblad, On the generators of quantum dynamical semigroups, Commun. Math. Phys. **48**, 119 (1976).

[2] V. Gorini, A. Kossakowski, and E. C. G. Sudarshan, Completely positive dynamical semigroups of $n$-level systems, J. Math. Phys. **17**, 821 (1976).

[3] H.-P. Breuer and F. Petruccione, *The Theory of Open Quantum Systems* (Oxford University Press on Demand, New York, 2002).

[4] T. Prosen, Third quantization: a general method to solve master equations for quadratic open Fermi systems, New J. Phys. **10**, 043026 (2008).

[5] T. Prosen, Spectral theorem for the Lindblad equation for quadratic open fermionic systems, J. Stat. Mech. (2010) P07020.

[6] T. Prosen and T. H. Seligman, Quantization over boson operator spaces, J. Phys. A: Math. Theor. **43**, 392004 (2010).

[7] T. Heinosaari, A. S. Holevo, and M. M. Wolf, The semigroup structure of gaussian channels, Quantum Info. Comput. **10**, 619 (2010).

[8] C. Guo and D. Poletti, Solutions for bosonic and fermionic dissipative quadratic open systems, Phys. Rev. A **95**, 052107 (2017).

[9] G. Dagvadorj, J. M. Fellows, S. Matyjaśkiewicz, F. M. Marchetti, I. Carusotto, and M. H. Szymańska, Nonequilibrium phase transition in a two-dimensional driven open quantum system, Phys. Rev. X **5**, 041028 (2015).

[10] D. Roscher, S. Diehl, and M. Buchhold, Phenomenology of first-order dark-state phase transitions, Phys. Rev. A **98**, 062117 (2018).

[11] N. Dogra, M. Landini, K. Kroeger, L. Hruby, T. Donner, and T. Esslinger, Dissipation-induced structural instability and chiral dynamics in a quantum gas, Science **366**, 1496 (2019).

[12] B. Buča and D. Jaksch, Dissipation induced nonstationarity in a quantum gas, Phys. Rev. Lett. **123**, 260401 (2019).

[13] E. I. Rodriguez Chiacchio and A. Nunnenkamp, Dissipation-induced instabilities of a spinor Bose-Einstein condensate inside an optical cavity, Phys. Rev. Lett. **122**, 193605 (2019).

[14] F. Carollo, E. Gillman, H. Weimer, and I. Lesanovsky, Critical behavior of the quantum contact process in one dimension, Phys. Rev. Lett. **123**, 100604 (2019).

[15] M. Jo, J. Lee, K. Choi, and B. Kahng, Absorbing phase transition with a continuously varying exponent in a quantum contact process: A neural network approach, Phys. Rev. Res. **3**, 013238 (2021).

[16] F. Carollo and I. Lesanovsky, Nonequilibrium dark space phase transition, Phys. Rev. Lett. **128**, 040603 (2022).

[17] S. Helmrich, A. Arias, G. Lochead, T. M. Wintermantel, M. Buchhold, S. Diehl, and S. Whitlock, Signatures of self-organized criticality in an ultracold atomic gas, Nature (London) **577**, 481 (2020).

[18] S. Diehl, A. Micheli, A. Kantian, B. Kraus, H. P. Büchler, and P. Zoller, Quantum states and phases in driven open quantum systems with cold atoms, Nat. Phys. **4**, 878 (2008).

[19] F. Verstraete, M. M. Wolf, and J. Ignacio Cirac, Quantum computation and quantum-state engineering driven by dissipation, Nat. Phys. **5**, 633 (2009).

[20] H. Weimer, M. Müller, I. Lesanovsky, P. Zoller, and H. P. Büchler, A Rydberg quantum simulator, Nat. Phys. **6**, 382 (2010).

[21] J. Cui, J. I. Cirac, and M. C. Bañuls, Variational matrix product operators for the steady state of dissipative quantum systems, Phys. Rev. Lett. **114**, 220601 (2015).

[22] J. Jin, A. Biella, O. Viyuela, L. Mazza, J. Keeling, R. Fazio, and D. Rossini, Cluster mean-field approach to the steady-state phase diagram of dissipative spin systems, Phys. Rev. X **6**, 031011 (2016).

[23] A. H. Werner, D. Jaschke, P. Silvi, M. Kliesch, T. Calarco, J. Eisert, and S. Montangero, Positive tensor network approach for simulating open quantum many-body systems, Phys. Rev. Lett. **116**, 237201 (2016).

[24] D. Jaschke, S. Montangero, and L. D. Carr, One-dimensional many-body entangled open quantum systems with tensor network methods, Quantum Sci. Technol. **4**, 013001 (2018).

[25] P. Silvi, F. Tschirsich, M. Gerster, J. Jünemann, D. Jaschke, M. Rizzi, and S. Montangero, The Tensor Networks Anthology: Simulation techniques for many-body quantum lattice systems, SciPost Phys. Lect. Notes 8 (2019).

[26] H. Weimer, A. Kshetrimayum, and R. Orús, Simulation methods for open quantum many-body systems, Rev. Mod. Phys. **93**, 015008 (2021).

[27] N. Yoshioka and R. Hamazaki, Constructing neural stationary states for open quantum many-body systems, Phys. Rev. B **99**, 214306 (2019).

[28] M. J. Hartmann and G. Carleo, Neural-network approach to dissipative quantum many-body dynamics, Phys. Rev. Lett. **122**, 250502 (2019).

[29] A. Nagy and V. Savona, Variational quantum Monte-Carlo method with a neural-network ansatz for open quantum systems, Phys. Rev. Lett. **122**, 250501 (2019).

[30] F. Vicentini, A. Biella, N. Regnault, and C. Ciuti, Variational neural-network ansatz for steady states in open quantum systems, Phys. Rev. Lett. **122**, 250503 (2019).

[31] M. Reh, M. Schmitt, and M. Gärttner, Time-dependent variational principle for open quantum systems with artificial neural networks, Phys. Rev. Lett. **127**, 230501 (2021).

[32] F. Vicentini, R. Rossi, and G. Carleo, Positive-definite parametrization of mixed quantum states with deep neural networks, arXiv:2206.13488.

[33] G. Vidal, Efficient classical simulation of slightly entangled quantum computations, Phys. Rev. Lett. **91**, 147902 (2003).

[34] G. Vidal, Efficient simulation of one-dimensional quantum many-body systems, Phys. Rev. Lett. **93**, 040502 (2004).

[35] U. Schollwöck, The density-matrix renormalization group in the age of matrix product states, Ann. Phys. **326**, 96 (2011).

[36] R. Orús, A practical introduction to tensor networks: Matrix product states and projected entangled pair states, Ann. Phys. (NY) **349**, 117 (2014).

[37] C. Lubich, I. V. Oseledets, and B. Vandereycken, Time integration of tensor trains, SIAM J. Numer. Anal. **53**, 917 (2015).

[38] J. Haegeman, C. Lubich, I. Oseledets, B. Vandereycken, and F. Verstraete, Unifying time evolution and optimization with matrix product states, Phys. Rev. B **94**, 165116 (2016).

[39] S. Paeckel, T. Köhler, A. Swoboda, S. R. Manmana, U. Schollwöck, and C. Hubig, Time-evolution methods for matrix-product states, Ann. Phys. (NY) **411**, 167998 (2019).

[40] R. Orús, Tensor networks for complex quantum systems, Nat. Rev. Phys. **1**, 538 (2019).

[41] J. I. Cirac, D. Pérez-García, N. Schuch, and F. Verstraete, Matrix product states and projected entangled pair states: Concepts, symmetries, theorems, Rev. Mod. Phys. **93**, 045003 (2021).

[42] P. Silvi, V. Giovannetti, S. Montangero, M. Rizzi, J. I. Cirac, and R. Fazio, Homogeneous binary trees as ground states of quantum critical Hamiltonians, Phys. Rev. A **81**, 062335 (2010).

[43] Y.-Y. Shi, L.-M. Duan, and G. Vidal, Classical simulation of quantum many-body systems with a tree tensor network, Phys. Rev. A **74**, 022320 (2006).

[44] N. Nakatani and G. K.-L. Chan, Efficient tree tensor network states (TTNS) for quantum chemistry: Generalizations of the density matrix renormalization group algorithm, J. Chem. Phys. **138**, 134113 (2013).

[45] F. A. Y. N. Schröder, D. H. P. Turban, A. J. Musser, N. D. M. Hine, and A. W. Chin, Tensor network simulation of multi-environmental open quantum dynamics via machine learning and entanglement renormalisation, Nat. Commun. **10**, 1062 (2019).

[46] L. Arceci, P. Silvi, and S. Montangero, Entanglement of formation of mixed many-body quantum states via tree tensor operators, Phys. Rev. Lett. **128**, 040501 (2022).

[47] Y. Ke, Tree tensor network state approach for solving hierarchical equations of motions, J. Chem. Phys. **158**, 211102 (2023).

[48] L. Tagliacozzo, G. Evenbly, and G. Vidal, Simulation of two-dimensional quantum systems using a tree tensor network that exploits the entropic area law, Phys. Rev. B **80**, 235127 (2009).

[49] V. Murg, F. Verstraete, O. Legeza, and R. M. Noack, Simulating strongly correlated quantum systems with tree tensor networks, Phys. Rev. B **82**, 205105 (2010).

[50] B. Kloss, D. R. Reichman, and Y. B. Lev, Studying dynamics in two-dimensional quantum lattices using tree tensor network states, SciPost Phys. **9**, 070 (2020).

[51] T. Felser, S. Notarnicola, and S. Montangero, Efficient tensor network ansatz for high-dimensional quantum many-body problems, Phys. Rev. Lett. **126**, 170603 (2021).

[52] S. Finazzi, A. Le Boité, F. Storme, A. Baksic, and C. Ciuti, Corner-space renormalization method for driven-dissipative two-dimensional correlated systems, Phys. Rev. Lett. **115**, 080604 (2015).

[53] R. Rota, F. Storme, N. Bartolo, R. Fazio, and C. Ciuti, Critical behavior of dissipative two-dimensional spin lattices, Phys. Rev. B **95**, 134431 (2017).

[54] R. Rota, F. Minganti, C. Ciuti, and V. Savona, Quantum critical regime in a quadratically driven nonlinear photonic lattice, Phys. Rev. Lett. **122**, 110405 (2019).

[55] G. Ceruti, C. Lubich, and D. Sulz, Rank-adaptive time integration of tree tensor networks, SIAM J. Numer. Anal. **61**, 194 (2023).

[56] F. Verstraete, J. J. García-Ripoll, and J. I. Cirac, Matrix product density operators: Simulation of finite-temperature and dissipative systems, Phys. Rev. Lett. **93**, 207204 (2004).

[57] M. Zwolak and G. Vidal, Mixed-state dynamics in one-dimensional quantum lattice systems: A time-dependent super-operator renormalization algorithm, Phys. Rev. Lett. **93**, 207205 (2004).

[58] A. Kshetrimayum, H. Weimer, and R. Orús, A simple tensor network algorithm for two-dimensional steady states, Nat. Commun. **8**, 1291 (2017).

[59] P. Kramer and M. Saraceno, *Geometry of the Time-Dependent Variational Principle in Quantum Mechanics*, Lecture Notes in Physics, Vol. 140 (Springer-Verlag, Berlin, 1981).

[60] C. Lubich, *From Quantum to Classical Molecular Dynamics: Reduced Models and Numerical Analysis*, Zurich Lectures in Advanced Mathematics (European Mathematical Society, Zürich, 2008).

[61] J. Haegeman, J. I. Cirac, T. J. Osborne, I. Pižorn, H. Verschelde, and F. Verstraete, Time-dependent variational principle for quantum lattices, Phys. Rev. Lett. **107**, 070601 (2011).

[62] G. Ceruti, C. Lubich, and H. Walach, Time integration of tree tensor networks, SIAM J. Numer. Anal. **59**, 289 (2021).

[63] G. Ceruti and C. Lubich, An unconventional robust integrator for dynamical low-rank approximation, BIT Numer. Math. **62**, 23 (2021).

[64] G. Ceruti, J. Kusch, and C. Lubich, A rank-adaptive robust integrator for dynamical low-rank approximation, Bit. Numer. Math. **62**, 1149 (2022).

[65] F. Benatti, F. Carollo, R. Floreanini, and H. Narnhofer, Quantum spin chain dissipative mean-field dynamics, J. Phys. A Math. Theor. **51**, 325001 (2018).

[66] F. Carollo and I. Lesanovsky, Exactness of mean-field equations for open Dicke models with an application to pattern retrieval dynamics, Phys. Rev. Lett. **126**, 230601 (2021).

[67] T. E. Lee, H. Häffner, and M. C. Cross, Antiferromagnetic phase transition in a nonequilibrium lattice of Rydberg atoms, Phys. Rev. A **84**, 031402(R) (2011).

[68] H. Weimer, Variational principle for steady states of dissipative quantum many-body systems, Phys. Rev. Lett. **114**, 040402 (2015).

[69] V. R. Overbeck, M. F. Maghrebi, A. V. Gorshkov, and H. Weimer, Multicritical behavior in dissipative Ising models, Phys. Rev. A **95**, 042133 (2017).

[70] M. Raghunandan, J. Wrachtrup, and H. Weimer, High-density quantum sensing with dissipative first order transitions, Phys. Rev. Lett. **120**, 150501 (2018).

[71] J. Jin, A. Biella, O. Viyuela, C. Ciuti, R. Fazio, and D. Rossini, Phase diagram of the dissipative quantum Ising model on a square lattice, Phys. Rev. B **98**, 241108(R) (2018).

[72] D. A. Paz and M. F. Maghrebi, Driven-dissipative Ising model: An exact field-theoretical analysis, Phys. Rev. A **104**, 023713 (2021).

[73] D. A. Paz and M. F. Maghrebi, Driven-dissipative Ising model: Dynamical crossover at weak dissipation, Europhys. Lett. **136**, 10002 (2021).

[74] J. Marino, Universality class of Ising critical states with long-range losses, Phys. Rev. Lett. **129**, 050603 (2022).

[75] F. B. Trigueros, T. Mendes-Santos, and M. Heyl, Mean-field theories are simple for neural quantum states, arXiv:2308.10934.

[76] M. Kac, G. E. Uhlenbeck, and P. C. Hemmer, On the van der Waals theory of the vapor-liquid equilibrium. I. Discussion of a one-dimensional model, J. Math. Phys. **4**, 216 (1963).

[77] N. Defenu, Metastability and discrete spectrum of long-range systems, Proc. Natl. Acad. Sci. USA **118**, e2101785118 (2021).

[78] K. Seetharam, A. Lerose, R. Fazio, and J. Marino, Dynamical scaling of correlations generated by short- and long-range dissipation, Phys. Rev. B **105**, 184305 (2022).

[79] B. A. Chase and J. M. Geremia, Collective processes of an ensemble of spin-1/2 particles, Phys. Rev. A **78**, 052101 (2008).

[80] B. Q. Baragiola, B. A. Chase, and J. M. Geremia, Collective uncertainty in partially polarized and partially decohered spin-$\frac{1}{2}$ systems, Phys. Rev. A **81**, 032104 (2010).

[81] P. Kirton and J. Keeling, Suppressing and restoring the Dicke superradiance transition by dephasing and decay, Phys. Rev. Lett. **118**, 123602 (2017).

[82] N. Shammah, S. Ahmed, N. Lambert, S. De Liberato, and F. Nori, Open quantum systems with local and collective incoherent processes: Efficient numerical simulations using permutational invariance, Phys. Rev. A **98**, 063815 (2018).

[83] G. Vidal, Classical simulation of infinite-size quantum lattice systems in one spatial dimension, Phys. Rev. Lett. **98**, 070201 (2007).

[84] M. Saffman, T. G. Walker, and K. Mølmer, Quantum information with Rydberg atoms, Rev. Mod. Phys. **82**, 2313 (2010).

[85] B. W. Bader, T. G. Kolda *et al.*, Tensor Toolbox for MATLAB, Version 3.2.1, www.tensortoolbox.org (2021).

[86] N. Vervliet, O. Debals, L. Sorber, M. Van Barel, and L. De Lathauwer, TENSORLAB 3.0, https://www.tensorlab.net/ (2016).

[87] D. Kressner and C. Tobler, Algorithm 941: HTUCKER–a MATLAB toolbox for tensors in hierarchical Tucker format, ACM Trans. Math. Softw. **40**, 1 (2014).